Exploring solar neutrino oscillation parameters with the liquid scintillator counter at Yemilab with a comparison to JUNO

Pouya Bakhti,[1,*] Meshkat Rajaee[1,†] Seon-Hee Seo,[2,3,‡] and Seodong Shin[1,4,§]

[1]*Laboratory for Symmetry and Structure of the Universe, Department of Physics,*
Jeonbuk National University, Jeonju, Jeonbuk 54896, South Korea
[2]*Center for Underground Physics, Institute for Basic Science,*
55 Expo-ro Yuseong-gu, Daejeon 34126, South Korea
[3]*Fermi National Accelerator Laboratory, Batavia, Illinois 60510, USA*
[4]*Particle Theory and Cosmology Group, Center for Theoretical Physics of the Universe,*
Institute for Basic Science (IBS), Daejeon 34126, South Korea

We investigate the sensitivities of the liquid scintillator counter (LSC) at Yemilab and JUNO to solar neutrino oscillation parameters, focusing on θ_{12} and Δm_{21}^2. We compare the potential of JUNO with LSC at Yemilab utilizing both reactor and solar data in determining those parameters. We find that the solar neutrino data of LSC at Yemilab is highly sensitive to θ_{12} enabling its determination with a higher precision compared to reactor experiments. Our study also reveals that if Δm_{21}^2 is larger, with a value close to the best-fit value of KamLAND, JUNO reactor data will have about two times better precision than the reactor LSC at Yemilab. On the other hand, if Δm_{21}^2 is smaller and closer to the best-fit value of solar neutrino experiments, the precision of the reactor LSC at Yemilab will be better than JUNO.

I. INTRODUCTION

Neutrinos are among the most elusive particles in the universe and hence studying their properties remains a key challenge in particle physics. One of the most intriguing phenomena in the study of neutrinos is neutrino oscillation, which refers to how neutrinos can transform between different flavors as they travel through space. The study of neutrino oscillations has led to important insights into the properties of neutrinos and the fundamental laws of the Universe. In particular, solar neutrino oscillations, which occur as neutrinos produced in the Sun travel to the Earth, have been the subject of intense research over the past few decades.

The solar neutrino problem arose from the observed deficit in the solar ν_e flux detected in various experiments such as Homestake [1], Super-Kamiokande [2–4], and gallium experiments [5,6]. In 2002, the Sudbury Neutrino Observatory (SNO) experiment [7] resolved this issue by confirming the accuracy of the Standard Solar Models using the neutral current signal, which measured all active neutrino flavors. By comparing these results with the ν_e flux obtained from the charged current signal, SNO provided compelling evidence of electron neutrino conversion into other flavors. Combining the SNO results with the data from the earlier experiments, along with the KamLAND reactor experiment [8], led to the discovery of the large mixing angle (LMA) Mikheyev-Smirnov-Wolfenstein (MSW) solution as the correct set of neutrino mixing parameters [9–11].

In recent years, the Borexino experiment using liquid scintillator detectors has achieved impressive low energy thresholds in the sub-MeV region at low background level. As a result, precise measurements of solar ^{7}Be neutrinos have been obtained, along with the observation of solar pep and pp neutrinos for the first time [12]. Moreover, Borexino has measured the CNO neutrinos for the first time, and more precise measurement of CNO neutrinos is crucial for solving solar metallicity problem. The observed results are consistent with the theoretical predictions of the MSW matter effect [9–11], providing further validation of this phenomenon in the context of neutrino oscillations. Indeed, there are still several key aspects of solar neutrinos that require further clarification. These include the need for improved determination of neutrino oscillation parameters, addressing the solar metallicity problem, and detailed analysis of the energy dependence in the low-energy region.

In this paper, we focus on the sensitivities of the liquid scintillator counter (LSC) at Yemilab to solar neutrino oscillation parameters. Yemilab is a recently built

[*]pouya_bakhti@jbnu.ac.kr
[†]meshkat@jbnu.ac.kr
[‡]shseo@fnal.gov
[§]sshin@jbnu.ac.kr

underground laboratory located at Mount Yemi in Jeongsun, Gangwon province, Korea. A few kton scale liquid scintillator neutrino detector, LSC, is considered to be installed in Yemilab in the near future, which would play an important role in the study of low-energy neutrinos. In this study, we analyze the detector's ability to detect solar neutrinos as well as reactor neutrinos from the Hanul Nuclear Power Plant located at Uljin, which is 65 km away from Yemilab.

Our main goal is to investigate the potential of LSC at Yemilab in precisely determining the solar neutrino oscillation parameters, namely θ_{12} and Δm_{21}^2. We analyze the detector's ability to detect solar neutrinos and reactor neutrinos, and compare our results with the potential of the Jiangmen Underground Neutrino Observatory (JUNO) [13], another leading neutrino detector in China, to determine these parameters. While the upcoming reactor experiment JUNO is expected to significantly enhance the measurement of certain oscillation parameters, such as solar parameters θ_{12} and Δm_{21}^2, it is crucial for solar neutrino experiments to independently verify these measurements. Precise determination of solar parameter Δm_{21}^2 can also play role in the determination of δ_{CP} in long-baseline experiments [14]. The forthcoming solar neutrino experiment LSC at Yemilab, which benefits from a lower energy threshold compared to JUNO and the ability to detect pp neutrinos with a larger fiducial volume compared to Borexino will provide higher statistics for determining the solar neutrino parameters. In this paper, we will elaborate on how LSC at Yemilab will be able to determine θ_{12} more precisely than JUNO. Furthermore, the combination of data from JUNO and LSC at Yemilab can offer an intriguing probe for the precise measurement of the solar parameters and hence possible investigation of physics beyond the standard 3-neutrino oscillation [15].

Our results reveal that LSC at Yemilab exhibits a unique sensitivity to θ_{12}, enabling precise determination of this parameter through the detection of solar neutrinos. Meanwhile, the value of Δm_{21}^2 can be determined with higher accuracy through the detection of reactor neutrinos. As we will elaborate more, if the value of Δm_{21}^2 is close to the best-fit value of KamLAND, JUNO will have the best sensitivity to determine it, while if Δm_{21}^2 is closer to the best-fit value of solar neutrino experiments, LSC at Yemilab can compete JUNO in measuring this value and provide a better measurement. Therefore, combining data from both experiments will yield the most accurate measurement of the solar neutrino oscillation parameters.

This paper is organized as follows. We revisit the physics of solar neutrino propagation from the Sun to the Earth in Sec. II and neutrino oscillation in reactors in Sec. III. The detailed information of LSC at Yemilab and JUNO is summarized in Sec. IV. Our main analysis results with proper plots are explained in Sec. V. Finally, we summarize our conclusions and discuss future prospects in Sec. VI.

II. SOLAR NEUTRINO PROPAGATION FROM THE SUN TO THE EARTH

Neutrino oscillation in matter is a phenomenon that occurs when neutrinos pass through a medium with a constant or varying density, such as the Sun or the Earth. The flavor of the neutrinos can change due to their interactions with the surrounding matter while propagating. This is known as MSW effect [9–11]. The MSW effect can have a significant impact on the observed solar neutrino flux depending on the density profile of the Sun. In the case of solar neutrinos, the flavor conversion is most sensitive to the mixing angle θ_{12} and the mass-squared difference Δm_{21}^2, which governs the oscillation between electron neutrinos and other neutrino flavors.

The evolution of a neutrino flavor state is described by the Schrödinger-like equation,

$$i\frac{d|\nu_f\rangle}{dx} = H|\nu_f\rangle = (H_0 + V)|\nu_f\rangle, \qquad (1)$$

where H is the total Hamiltonian, H_0 is the vacuum Hamiltonian, and $V = \mathrm{diag}(V_e, 0, 0)$ is the diagonal matrix of matter potentials with $V_e = \sqrt{2}G_F n_e$. Here, G_F is the Fermi constant and n_e is the number density of electrons. The parameter x denotes the oscillation length approximately the same as the propagation time. Note that the Hamiltonian is not diagonal in the flavor basis.

The evolution of flavor neutrino states is described in terms of the instantaneous eigenstates of the Hamiltonian in matter, denoted as $|\nu_m\rangle \equiv (\nu_{1m}, \nu_{2m}, \nu_{3m})^T$. The relationship between these eigenstates and the flavor states is expressed through the mixing matrix in matter, denoted as U_m,

$$|\nu_f\rangle = U_m|\nu_m\rangle. \qquad (2)$$

The matrix U_m diagonalizes the Hamiltonian,

$$U_m^\dagger H U_m = \mathrm{diag}(H_{1m}, H_{2m}, H_{3m}), \qquad (3)$$

where H_{im} are the eigenvalues of the Hamiltonian.

The propagation and flavor evolution of solar neutrinos can be studied in three distinct stages: (1) propagation inside the Sun; (2) propagation from the Sun to the Earth; (3) propagation inside the Earth. When an electron neutrino is produced in the core of the Sun, it propagates through space inside the Sun as a combination of different neutrino mass states, known as eigenstates of the Hamiltonian in Eq. (1).

While propagating through the space between the Sun and the Earth, the high energy neutrinos lose coherence and no oscillations occur.[1] However, as they enter the Earth, the

---

[1]The low-energy neutrinos have already lost the coherence inside the Sun.

mass states split into the eigenstates of the Hamiltonian in the Earth's matter and begin to oscillate as they travel through the Earth towards a detector. In the following, we will elaborate on each phase independently.

As solar neutrinos travel from their production point in the Sun to the Earth, the wave packets associated with different mass eigenstates will separate due to their distinct group velocities, leading to the loss of propagation coherence. Moreover, each wave packet spreads as a consequence of having different momenta. However, it is important to note that although the spread is present, it remains smaller compared to the separation between the eigenstates [16]. Thus, this spreading does not significantly impact the coherence condition. As a result, the fluxes of the mass eigenstates of solar neutrinos arrive at the Earth incoherently. The probability of detecting a ν_e at arrival time t on the *surface* of the Earth is given by [17]

$$P_{ee}^{\text{sur}} = |\langle \nu_e | \nu(t) \rangle|^2 = \sum_j |U_{ej}^m(n_e^0)|^2 |U_{ej}|^2, \qquad (4)$$

where $U_{ej}^m(n_e^0)$ are the elements of mixing matrix in the production point with density n_e^0. Using the standard parametrization of the mixing matrix, P_{ee}^{sur} can be written as [17,18]

$$P_{ee}^{\text{sur}} = \frac{1}{2} c_{13}^2 c_{13}^{m2} (1 + \cos 2\theta_{12} \cos 2\theta_{12}^m) + s_{13}^2 s_{13}^{m2}. \quad (5)$$

The 1–2 mixing angle θ_{12}^m is determined by

$$\cos 2\theta_{12}^m = \frac{\cos 2\theta_{12} - c_{13}^2 \epsilon_{12}}{\sqrt{(\cos 2\theta_{12} - c_{13}^2 \epsilon_{12})^2 + \sin^2 2\theta_{12}}}, \quad (6)$$

where

$$\epsilon_{12} \equiv \frac{A_{CC}}{\Delta m_{21}^2}, \qquad (7)$$

with $A_{CC} = 2V_e E$. Notice that matter effect is important for high energies where ϵ_{12} is not negligible.

Finally, at the time solar neutrinos reach the Earth's surface, they undergo a flavor conversion due to the presence of matter. The probability of detecting an electron neutrino now becomes,

$$P_{ee} = \sum_j |U_{ej}^m(n_e^0)|^2 \cdot P_{je}, \qquad (8)$$

where P_{je} are the probabilities of *oscillatory* transitions $\nu_j \to \nu_e$ in the Earth matter [18,19], while $|U_{ej}|^2$ in Eq. (4) is the square of the *fixed* component of the mixing matrix.

Please note that the dependence on the day-night asymmetry becomes crucial at higher energies ($E > 5$ MeV) for [8]B solar neutrinos. Experiments with larger fiducial volumes,

such as Hyper-Kamiokande (HK) and DUNE, demonstrate superior sensitivity to the day-night asymmetry compared to JUNO and Yemilab. Moreover, the day-night asymmetry shows significant sensitivity to the measurement of Δm_{21}^2 in general [20]. The significant uncertainties in current Earth models can greatly impact the sensitivity of Δm_{21}^2 measurements. Different 3D Earth models present inconsistencies, particularly in the East Asian region where JUNO and HK are situated [18].

III. NEUTRINO OSCILLATION IN REACTORS

The mechanism of neutrino oscillation can be explained by the fact that the three neutrino flavors are not distinct states of definite mass, but are quantum mechanical superpositions of three different mass states. As a result, as neutrinos travel through (some) space, they can undergo a transformation among those different mass eigenstates, leading to oscillations into different flavor eigenstates at the time of detection. The Pontecorvo-Maki-Nakagawa-Sakata (PMNS) matrix, is a unitary matrix that describes the mixing of neutrino flavor states (electron, muon, and tau) with the neutrino mass eigenstates (ν_1, ν_2, and ν_3). The PMNS matrix can be parametrized with three mixing angles, θ_{12}, θ_{13}, and θ_{23} and one δ_{CP} phase if the neutrinos are Dirac fermions.

The probability of a produced α flavor neutrino ν_α being detected as a β flavor neutrino ν_β is given by

$$P_{\nu_\alpha \to \nu_\beta}(t) = \sum_{k,j} U_{\alpha k}^* U_{\beta k} U_{\alpha j} U_{\beta j}^* \exp\left(-\frac{i\Delta m_{kj}^2 L}{2E}\right), \quad (9)$$

where E is the energy of the neutrino, $U_{\alpha k}$ are the elements of the PMNS matrix and Δm_{ij}^2 is the squared-mass differences between mass eigenstate of i and j, and L is the baseline. As stated in the previous section, the presence of matter can significantly affect the neutrino oscillations, particularly for neutrinos with high energies and high matter density where $\epsilon_{12} \equiv A_{CC}/\Delta m_{21}^2$ is significant. The matter effect is not important for reactor neutrinos with energies of $\mathcal{O}(\text{MeV})$ which propagate through the Earth crust with density of 2.6 gr/cm^3, due to the fact that ϵ_{12} is negligible.

In reactor neutrino experiments, electron antineutrinos ($\bar{\nu}_e$) are produced and detected. The oscillation probability $P(\bar{\nu}_e \to \bar{\nu}_e)$ is expressed as follows:

$$
\begin{aligned}
P(\bar{\nu}_e \to \bar{\nu}_e) &= ||U_{e1}|^2 + |U_{e2}|^2 e^{i\Delta_{21}} + |U_{e3}|^2 e^{i\Delta_{31}}|^2 \\
&= |c_{12}^2 c_{13}^2 + s_{12}^2 c_{13}^2 e^{i\Delta_{21}} + s_{13}^2 e^{i\Delta_{31}}|^2 \\
&= c_{13}^4 \left(1 - \sin^2 2\theta_{12} \sin^2 \frac{\Delta_{21}}{2}\right) + s_{13}^4 \\
&\quad + 2s_{13}^2 c_{13}^2 [\cos \Delta_{31}(c_{12}^2 + s_{12}^2 \cos \Delta_{21}) \\
&\quad + s_{12}^2 \sin \Delta_{31} \sin \Delta_{21}], \qquad (10)
\end{aligned}
$$

where $\Delta_{ij} = \Delta m_{ij}^2 L/(2E_\nu)$. For reactor experiments with $\mathcal{O}(1 \text{ km})$ baseline, such as Daya Bay [21], RENO [22], or Double-CHOOZ [23], the value of Δm_{21}^2 can be effectively approximated as zero due to the relatively small baseline length. Consequently, this approximation results in reduced sensitivity when measuring the mixing angle θ_{12}. However, it's important to note that these experiments retain their sensitivity to larger values of Δm_{21}^2 [24,25]. For neutrino oscillation with one km baseline reactor neutrinos, the key parameters are θ_{13} and Δm_{31}^2. On the other hand, the value Δ_{21} can be non-negligible in longer baseline experiments such as LSC at Yemilab (from Hanul power plant), JUNO, and KamLAND. Reactor neutrinos offer significant advantages for the study of neutrino oscillation due to their large flux and well-characterized energy spectrum. Moreover, the relatively short baselines between reactor neutrino sources and detectors, typically spanning tens of kilometers, make them exceptionally well-suited for precise measurements of oscillation parameters. Reactor neutrino experiments with shorter baselines, such as Daya Bay and RENO have successfully delivered precise measurements of the mixing angle θ_{13} [21,22]. On the other hand, experiments with longer baselines hold the potential to unravel crucial information regarding other significant oscillation parameters, including θ_{12}, Δm_{21}^2, and Δm_{31}^2. In the following section, we will provide detailed explanations of the two reactor experiments utilized in this study; LSC at Yemilab and JUNO.

IV. DETAILS OF LSC AT YEMILAB AND JUNO EXPERIMENTS

In this chapter, we will elaborate on the experiments we have employed. To detect reactor and solar neutrinos, charged current (CC) reaction inverse beta decay on protons and elastic neutrino scattering are used, respectively.

Yemilab is situated 1 km deep in Handuk iron mine, Jeongsun-gun, Gangwon-do, Korea. The primary research programs to start in 2023–2024 at Yemilab are the dark matter direct detection with COSINE-200 and neutrinoless double-beta decay search with AMoRE-II. LSC is a multipurpose detector covering from astroparticle to particle physics, and if funded, its main physics would be to precisely measure solar neutrinos, search for sterile neutrinos using IsoDAR and/or radioactive source(s), and search for dark photons using a linear accelerator (LINAC) [26].

One of the key advantages of a liquid scintillator detector LSC is its remarkable ability to detect a wide range of neutrino energies, spanning from a few 100 keV to several GeV. This exceptional energy range makes it an ideal detector for studying solar neutrinos, which exhibit energies ranging from a few 100 keV to less than twenty MeV. The detector consists of a 2.26 kton linear alkyl-benzenes (LAB)-based liquid scintillator housed within an acrylic cylinder vessel with dimensions of 15 m in diameter and

15 m in height. The buffer region surrounding the scintillator is filled with mineral oil, weighing 1.14 ktons, contained within a stainless steel vessel measuring 17 m in diameter and 17 m in height. Additionally, the veto region is filled with purified water, amounting to 2.41 ktons, in a stainless steel vessel (or no vessel but a lining of the cavity) with dimensions of 20 m in diameter and 20 m in height.

Yemilab is situated approximately 65 km away from the Hanul Nuclear Power Plant at Uljin, Gyeongsangbuk-do, South Korea. This enables Yemilab to utilize reactor neutrinos emitted by the power plant as a valuable calibration source for the neutrino detectors. By detecting and analyzing both solar and reactor neutrinos, LSC at Yemilab has an excellent capability of investigating neutrino oscillations to accurately determine the oscillation parameters of solar neutrinos, namely θ_{12} and Δm_{21}^2. More details on LSC is in Ref. [26].

In our analysis of reactor neutrino detection, we have considered a fiducial volume of 2 kton for LSC. The reactor complex at Hanul nuclear power plant consists of eight reactors, namely Hanul-1 to Hanul-6, and Shin-Hanul-1 and Shin-Hanul-2 (from December 2023), with a total thermal power output of 24.816 GW$_{\text{th}}$. Among these reactors, Hanul-1 and Hanul-2 have a power output of 2.775 GW$_{\text{th}}$ each, while Hanul-3 to Hanul-6 have a power output of 2.825 GW$_{\text{th}}$ each. In addition to these reactors, the complex includes two new reactors, Shin-Hanul-1 and Shin-Hanul-2, with a power output of 3.983 GW$_{\text{th}}$ each [26]. The distance between LSC at Yemilab and the reactors is approximately 65 km. LSC will have 2 times better shielding of muons due to more overburden compared to JUNO and 10 times smaller volume. This results in 20 times fewer cosmogentic background events in LSC compared to JUNO. Thus, the signal to cosmogentic background ratio will be improved by a factor 2. Other background sources, such as accidental, geoneutrino, and $^{13}\text{C}(\alpha, n)^{16}\text{O}$ events, are considered to have an equal ratio to the signal for both JUNO and Yemilab.

Background in reactor neutrino experiments is typically categorized into accidental and correlated background components. The correlated background primarily arises from fast neutrons, ^9Li and ^8He beta decays, and can be induced by cosmic muons. However, it is essential to note that correlated background can also stem from alpha reactions, which are entirely independent of cosmic muons. Additionally, the background attributed to muons is not inherently irreducible.

Fast neutrons originating from interactions caused by cosmic muons outside the detector (and veto) will be notably better shielded in JUNO due to its significantly larger mass. In JUNO, implementing a relatively modest cut on the fiducial volume proves effective, whereas LSC faces more challenges in this regard. Accidental background events are predominantly influenced by intrinsic radioactivity rather than cosmic muons.

Consequently, the ultimate background levels achieved in both experiments, JUNO and LSC, will hinge on various parameters, many of which are currently unknown. Factors such as shielding efficiency, fiducial volume selection, and the intrinsic radioactivity of materials play critical roles in shaping the background landscape. The comparison between JUNO and LSC underscores the intricate interplay of these parameters, ultimately determining the success in achieving low background levels in each experiment.

We have assumed a detector efficiency of 90%, normalization uncertainty of 0.8%, energy calibration error of 0.5%, and have adopted other experimental details consistent with Ref. [27]. To carry out our analysis we have used GLoBES software [28,29]. For the statistical inferences, we have considered the Asimov dataset approximation.

In our analysis of solar neutrinos at LSC, the energy threshold is taken as 0.18 MeV. This is because the intrinsic ^{14}C background events below 0.18 MeV are huge, several orders of magnitude larger than pp neutrino signal. Above 0.18 MeV, dominant backgrounds are cosmogenic muon-induced backgrounds and internal and environmental radioactive backgrounds. To account for these backgrounds, we have adopted the same background modeling approach as the Jinping experiment [30]. It should be noted that we did not take into account the ^{210}Po background, which is specific of Borexino. In our analysis of solar neutrinos, we have conservatively assumed a fiducial volume of 1 kton for LSC at Yemilab.

^{14}C is a carbon isotope characterized by a radioactive beta decay lifetime of $\tau = 8266.6$ yr and Q-value of 156.5 keV. The ^{12}C to ^{14}C ratio exhibits temporal variations. In petroleum reservoirs, this ratio reflects the average age of the organisms that contributed to oil formation, showing variability across different reservoirs. Remarkably, this ratio remains indifferent to the chemical composition or derivatives of the oil. In the Borexino experiment, after purification, the concentration of ^{14}C was 2.7×10^{-18} gr/gr [31]. While it is possible for the concentration of ^{14}C to reach levels as low as 10^{-20} or lower in extracted oil, producing a material with a ^{14}C concentration below 10^{-18} gr/gr presents substantial technical challenges. These challenges include the risk of contamination with environmental carbon during the production of liquid scintillator [32].

The activity of ^{14}C in a detector with a mass of m_{det}, ^{14}C concentration C, is expressed as

$$A = \frac{m_{\text{det}} C N_A}{M \tau}, \tag{11}$$

here, M represents the molar mass of ^{14}C (M = 14), N_A is Avogadro's number ($N_A = 6.022 \times 10^{23}$), and τ is the lifetime of ^{14}C. For Borexino, equipped with a one-kiloton detector and a concentration of 2.7×10^{-18} gr/gr, the resulting activity of ^{14}C is 5.3×10^3 Bq. For this concentration, the ratio of pp events to ^{14}C beta decay is 3×10^{-6}.

It should be noted that this ratio remains unaffected by the detector's mass, as both the number of signal and background events linearly increase with detector mass.[2] Consequently, the detection of pp events below 156.5 keV is not feasible for carbon-based scintillator detectors even with perfect energy resolutions. Our estimations show that considering a perfect energy resolution and assuming an energy threshold of 0.156 MeV, we can detect 70% of the pp neutrinos. Assuming an energy resolution similar to that of Borexino ($\sigma_E/E \approx 1/\sqrt{500 \frac{E}{\text{MeV}}} \approx 4.5\%$) and an energy threshold of 0.2 MeV, we can detect approximately 42% of the pp neutrinos. Moreover, with an energy resolution of $\sigma_E/E \approx 1/\sqrt{200 \frac{E}{\text{MeV}}} \approx 7\%$, we can detect around 30% of the events. In our calculations, we have assumed an energy resolution of $\sigma_E/E \approx 1/\sqrt{1000 \frac{E}{\text{MeV}}} \approx 3.2\%$ and an energy threshold of 0.18, resulting in the detection of 50% of the pp neutrinos.

In instances where more than one ^{14}C event occurs within the same time window of detection of pp neutrinos, these events are identified as single events with the summation of energies, a phenomenon referred to as pile-up events. The number of pile-up events is described by

$$N_{\text{pile-up}} = \frac{e^{-A\delta t} A^n \delta t^{n-1}}{(n-1)!}, \tag{12}$$

where A is activity of the ^{14}C given in Eq. (11), δt is the time window, and n is number of coincidence of events within the same time window. In the case of scintillator detectors designed for detecting pp neutrinos, the typical δt falls within a range of a few hundred nanoseconds. For ^{14}C activity, $A\delta t \ll 1$, and $e^{-A\delta t}$ is approximately equal to one. Consequently, the number of double pile-up events, representing the coincidence of two events in a detector's time window, is given by $A^2\delta t$. This implies that the ratio of double pile-up events to pp events increases linearly with the size of the detector. For ^{14}C concentrations on the order of 10^{-18} gr/gr, the ratio for one- and ten-kiloton detectors is around order of ten and a hundred, respectively. For detectors smaller than 100 tons, the rate of pp neutrinos is larger than double pile-up events [33].

In the scenario involving three pile-up events, the number of pp neutrino events is three orders of magnitude larger than that of pile-up events for a one-kiloton detector. Conversely, for a ten-kiloton detector, the numbers of pp neutrino events and three pile-up events are of comparable magnitude. With four pile-up events, the ratio of pp neutrino events to the pile-up events is 10^6 and 10^3 for one-kiloton and ten-kiloton detectors, respectively. Our

---

[2]However, in the case of pile-up events, which will be discussed later, the ratio of signal to background increases with detector mass.

analysis focuses solely on double pile-up events, as higher-order pile-up events become negligible for a two-kiloton detector after background rejection.

Distinguishing between single pp solar events and ^{14}C double pile-up events is possible through spatial and temporal information. However, the improvement in double pile-up background rejection comes at the cost of reduced pp signal efficiency. The balance between background rejection and signal efficiency is experiment-specific, and estimating these parameters goes beyond the scope of this work. Reference [34], considering different discrimination algorithms of pp neutrinos and double pile-up events, for a specific configuration detector indicates 90% to 95% background rejection with over 90% signal efficiency. For a one-kiloton detector with such characteristics, the number of pp signal and double pile-up background are comparable, or the number of pp events may even exceed the background. However, for ten-kiloton detectors, achieving more than 99% background rejection is necessary. Signal efficiency, depending on the detector details, may drop below 50 percent or even less than 10% for background rejection of more than 99%. Consequently, detecting pp neutrinos with a comparable number of double pile-up events poses a substantial challenge, requiring additional efforts and studies.

For smaller detectors, such as the one or two kiloton detector at Yemilab or Jinping, double pile-up event rejection is more feasible. The ratio of double pile-up to pp neutrinos is an order of magnitude smaller than that for JUNO, considering similar time windows and ^{14}C concentrations. In our analysis, we adopt the spectrum shape of double ^{14}C pile-up events from Ref. [34] for the case of LSC at Yemilab. For JUNO, we do not consider the detection of pp neutrinos. However, it is important to note that, in principle, detecting pp neutrinos at JUNO might be possible and warrants further investigations.

The determination of the detector's fiducial volume is mainly impacted by environmental contamination and spatial resolution. The spatial resolution, governed by the number of photomultiplier tubes (PMTs), is pivotal for distinguishing events occurring within the detector from those originating outside. The penetration of externally produced particles is contingent upon their energy, and the capability to differentiate such events amid internal detector events relies on the spatial resolution. As in the case of Jinping, we have also assumed that the fiducial volume of the detector for the detection of solar neutrinos is half of the liquid scintillator mass [30].

JUNO is an advanced liquid scintillator detector situated in southern China, at a distance of approximately 53 km from the Yangjiang and Taishan nuclear power plants. The JUNO detector is composed of a central acrylic sphere measuring 35 m in diameter, which is filled with 20 kton of liquid scintillator. Furthermore, 20,000 (25,600) 20-inch (3-inch) PMTs are mounted on a stainless steel lattice structure outside the acrylic sphere vessel, enabling the detection of light emitted by neutrino interactions within the scintillator [13].

One of the primary goals of JUNO is to investigate neutrino oscillations utilizing the reactor neutrinos generated by nearby nuclear power plants. Reactor neutrinos possess a well-characterized energy spectrum and flavor composition, rendering them an exceptional resource for studying neutrino oscillations. The key focus of JUNO is to determine the mass ordering of neutrinos, a crucial aspect in understanding their fundamental properties. Additionally, JUNO offers the advantage of measuring the oscillation parameters θ_{12} and Δm_{21}^2 with remarkable precision. With its substantial detector size and close proximity to the nuclear power plants, JUNO is anticipated to achieve a statistical uncertainty on $\sin^2 2\theta_{12}$ that is approximately four times superior to the current best measurement achieved by the KamLAND experiment [13].

In addition to reactor neutrinos, JUNO is also sensitive to solar, atmospheric, and supernova neutrinos. With its exceptional detection efficiency, outstanding energy resolution (ranging from 3% to 3.5%), and minimal background levels, the JUNO detector serves as a powerful instrument for scrutinizing neutrinos from various sources. While JUNO may not detect the lowest energy pp neutrinos, it possesses the capability to measure the higher energy ^{8}B neutrinos with a threshold of 2 MeV. Moreover, JUNO is actively exploring methods to mitigate the background originating from ^{210}Bi in order to detect ^{7}Be neutrinos, which encompass energies of 0.384 MeV and 0.862 MeV [13].

The study of solar neutrinos stands as a crucial component of JUNO's scientific agenda. By precisely measuring the flux and energy spectrum of solar neutrinos, JUNO can furnish invaluable insights into the fusion processes that energize the Sun, as well as neutrino oscillations transpiring within the high-density environment of the solar interior. In particular, JUNO holds the potential to make substantial advancements in our comprehension of the solar abundance problem and other discrepancies, which pertains to the persistent discrepancy between the anticipated and observed flux of solar neutrinos. Through the precise detection of ^{8}B neutrinos and the measurement of other solar neutrino fluxes, JUNO may provide better constraints on solar models and neutrino oscillation parameters. JUNO is also expected to detect a small number of hep neutrinos, which are produced by a rare fusion process in the Sun. The detection of hep neutrinos, which have a maximum energy of approximately 18.8 MeV, will provide a unique probe of the high-energy neutrino physics of the solar core.

For the analysis of JUNO reactor neutrinos, we have adopted the same experimental details as described in Refs. [35,36]. We have assumed a selection efficiency of 73% for electron anti-neutrino [13]. The primary sources of background in our analysis include cosmogenic background [37], accidental background, geoneutrino background, and

TABLE I.   The fiducial volume we considered for the analysis and the main backgrounds for each solar and reactor neutrino in LSC at Yemilab and JUNO.

Experiment	Fiducial volume considered	Background
JUNO (reactor)	20 kton	Cosmogenic background, accidental background, Geoneutrino background, $^{13}C(\alpha, n)^{16}O$
JUNO (Solar ^{7}Be)	20 kton	Intrinsic radioactive background
JUNO (Solar ^{8}B)	16 kton	Cosmogenic backgrounds, intrinsic radioactive background, and neutron capture
LSC at Yemilab (reactor)	2 kton	Cosmogenic background, accidental background, Geoneutrino background, $^{13}C(\alpha, n)^{16}O$
LSC at Yemilab (solar)	1 kton	Cosmogenic backgrounds, intrinsic radioactive background

the contribution from $^{13}C(\alpha, n)^{16}O$. We have considered a flux normalization uncertainty of 5%. The scintillator detector employed in JUNO will have a fiducial mass of 20 kton and an energy resolution of 3% is assumed in our analysis [13].

In the analysis of JUNO low-energy solar neutrinos, we have considered the detection of ^{7}Be neutrinos and a very small contribution from pp neutrinos with electron kinetic energy greater than 0.2 MeV. Below 0.2 MeV, the presence of a significant ^{14}C background poses a challenge as it is several orders of magnitude higher than the solar neutrino signals. The number of events from other low-energy solar neutrinos is much smaller compared to the background. The main sources of background at low energies include ^{210}Bi, ^{85}Kr, ^{40}K, ^{14}C, ^{238}U, ^{232}Th, and ^{11}C. In our analysis, we have considered two scenarios for the background; an ordinary case where the background is reduced compared to KamLAND's solar neutrino detection, and an ideal radiopurity assumption that is comparable to the lower background observed in Borexino phase I. For the detection of high-energy ^{8}B neutrinos, the main sources of background are cosmogenic isotopes such as ^{11}C, ^{10}C, and ^{11}Be. Below 3.5 MeV, both ^{11}C and ^{10}C contribute a large number of background events. Above 3.5 MeV, the only significant source of background is ^{11}Be, which may be half of the number of events or comparable to the ^{8}B solar neutrino signal [13,38]. Note that, measurements of pp and solar ^{7}Be neutrinos should remain unaffected by cosmic muons. This is because short-lived isotopes can be promptly vetoed by detecting muons in the veto system. Other isotopes like ^{11}C and ^{10}C, which pose a risk, produce signals significantly exceeding 1 MeV and are only problematic for measurements involving pep, CNO, and ^{8}B neutrinos.

Additionally, neutron captures on steel produce gamma rays with energies of 6 MeV and 8.5 MeV, which can penetrate the center of the JUNO detector [13]. To mitigate this background, reducing the fiducial volume to less than half of the detector's size is necessary. In our analysis, we have considered a 20 kton detector for the detection of low-energy solar neutrinos (^{7}Be neutrinos), and a 16 kton

detector for the detection of ^{8}B neutrinos. We have assumed efficiencies of 100% and 50% for ^{7}Be and ^{8}B neutrinos, respectively [38]. As we will elaborate on, our calculations demonstrate that for the detection of hep neutrinos with electron kinetic energies greater than 14.8 MeV, using a 20 kton fiducial volume, we anticipate six events after ten years of data collection while we expect the detection of only one ^{8}B solar neutrino in this energy range. However, the actual fiducial volume could be smaller than this. The details of the fiducial volume we considered for the analysis and the main backgrounds for each solar and reactor neutrino are tabulated in Table I.

V. RESULTS

In this section, we present our analysis results of the sensitivities of LSC at Yemilab and JUNO on the solar neutrino oscillation parameters. First, we will discuss the oscillation probabilities for reactor neutrinos and solar neutrinos. Subsequently, we will provide the number of events for the reactor neutrino data and solar neutrino data. Finally, we will illustrate the sensitivities of the two experiments on solar neutrino oscillation parameters, specifically focusing on Δm^2_{21} and θ_{12}. In our analysis, we focus on the survival probabilities of electron (anti-)neutrinos due to the exclusive production of electron (anti)neutrinos by both reactor neutrinos and solar neutrinos. The baselines for reactor neutrinos are set to be 52.5 km for JUNO and 65 km for LSC at Yemilab, respectively. To determine the oscillation parameters, we adopt the current best-fit values obtained from the KamLAND data; $\Delta m^2_{21} = 7.54 \times 10^{-5}$ eV^2 and $\sin^2 \theta_{12} = 0.316$. Additionally, we consider the best fit values from the combination of Super-Kamiokande (SK) and SNO solar data, which yield $\Delta m^2_{21} = 6.11 \times 10^{-5}$ eV^2 and $\sin^2 \theta_{12} = 0.306$ [39].

A. Oscillation probabilities and the expected number of events

Figure 1 shows the electron neutrino survival probabilities P_{ee} as a function of energy for two different baselines.
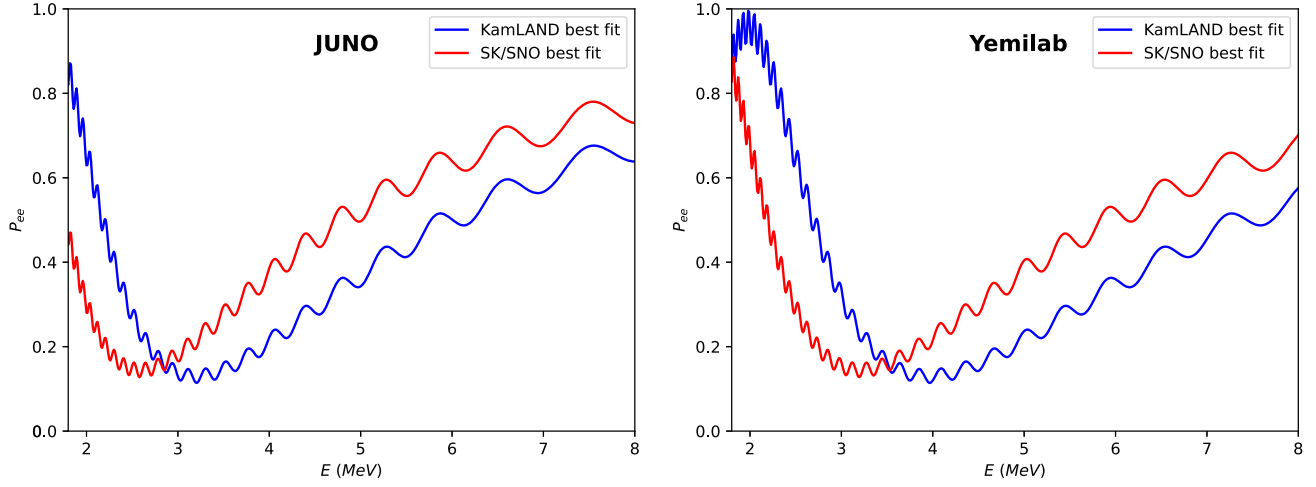
FIG. 1.   Reactor neutrino survival probability, P_{ee}, as a function of neutrino energy for different values of solar parameters, Δm_{21}^2 and θ_{12}. The blue curves correspond to the best-fit values of KamLAND data, while the red curves correspond to the best-fit values of SK/SNO solar neutrino data. These curves represent the oscillation probabilities for baselines of 52.5 km (JUNO baseline) and 65 km (Yemilab baseline).

The blue curves correspond to the best-fit values of KamLAND data ($\Delta m_{21}^2 = 7.54 \times 10^{-5}$ eV^2 and $\sin^2\theta_{12} = 0.316$), while the red curves correspond to the best-fit values of SK/SNO data ($\Delta m_{21}^2 = 6.11 \times 10^{-5}$ eV^2 and $\sin^2\theta_{12} = 0.306$) [39]. As expected, the oscillation probabilities at LSC at Yemilab (65 km) and JUNO (52.5 km) exhibit distinct patterns due to the difference in baselines. The curves demonstrate that the electron neutrino survival probabilities at both baselines are influenced by the values of Δm_{21}^2 and θ_{12}. In our analysis, we assume a normal mass ordering and fix θ_{13} at the best-fit value of the Daya Bay experiment [40] and the value of Δm_{31}^2 to the best-fit value of the nu-fit analysis [20].

Figure 2 depicts the electron neutrino survival probabilities P_{ee} as a function of energy for solar neutrinos. We have taken into account various aspects related to solar neutrinos and the Sun, such as the density of the Sun and the distribution functions of neutrino production in the pp chains and CNO cycle, as described in Ref. [41]. The blue curves correspond to the best-fit values of KamLAND data ($\Delta m_{21}^2 = 7.54 \times 10^{-5}$ eV^2 and $\sin^2\theta_{12} = 0.316$), while the red curves correspond to the best-fit values of SK/SNO solar neutrino data ($\Delta m_{21}^2 = 6.11 \times 10^{-5}$ eV^2 and $\sin^2\theta_{12} = 0.306$) [39]. Note that the quantity P_{ee} represents the ratio of the averaged electron neutrino flux to the sum of all fluxes ($P_{ee} = \frac{\phi_{CC}}{\phi_{NC}}$). The data points are set to the best-fit values of Borexino results for the pp, ^{7}Be, pep, and ^{8}B fluxes, assuming the GS98 solar model [42]. The error bars indicate the statistical uncertainties in the ten years of running LSC at Yemilab plus predicted flux uncertainties [43]. Notice that if Δm_{21}^2 lies within the range $5 \times 10^{-5} < \Delta m_{21}^2 < 9 \times 10^{-5}$, the oscillation of pp neutrinos is primarily sensitive to the value of θ_{12}.

This sensitivity arises due to vacuum oscillations occurring in the energy range of approximately 0.2 MeV to 0.4 MeV [see Eq. (5)]. In the case of ^{7}Be neutrinos, the matter effect becomes more significant due to their higher energy. As a result, they exhibit sensitivity to both Δm_{21}^2 and θ_{12}. Also, as can be observed from Fig. 2, ^{7}Be is close to the vacuum solution with only a small deviation, dependent on the Δm_{21}^2. Moreover, the resonance occurs specifically for ^{8}B neutrinos, making them essential for precise measurements of both Δm_{21}^2 and θ_{12}.
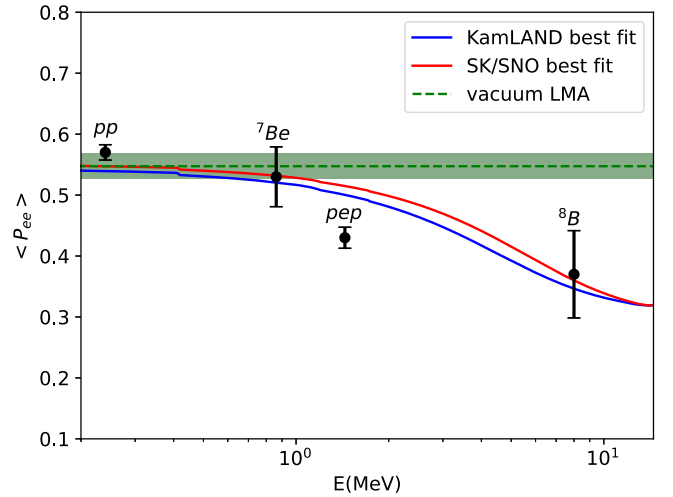

FIG. 2.   Solar neutrino survival probability, P_{ee}, as a function of neutrino energy for different values of Δm_{21}^2 and θ_{12}, corresponding to the best-fit values of KamLAND data (blue curve) and SK/SNO solar neutrino data (red curve). Data points are expected from LSC at Yemilab for ten years of operation (statistical error plus predicted flux uncertainties [43] are included, using Borexino-measured values [44] as the central values.
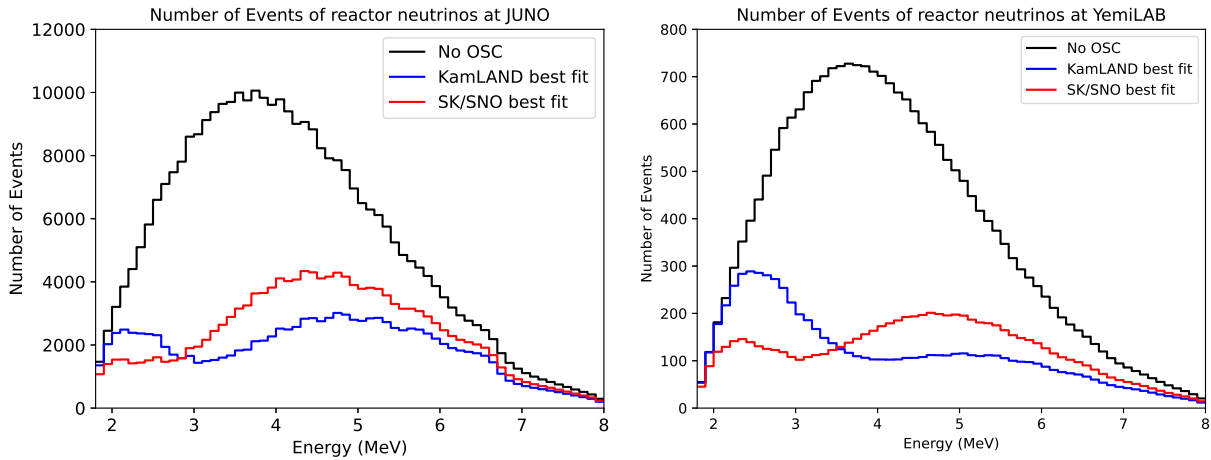
FIG. 3.   The number of events per bin (0.1 MeV) as a function of energy for two different sets of Δm_{21}^2 and θ_{12}. The blue curves correspond to the best-fit values of Kamland data, while the red curves correspond to the best-fit values of SK/SNO solar neutrino data. The calculations are based on a data-taking period of ten years and consider two different baselines; 52.5 km, corresponding to the JUNO baseline, and 65 km, corresponding to the Yemilab baseline.

We present the number of events of reactor neutrinos detectable by JUNO and LSC at Yemilab in Fig. 3. The black curve represents the case of no-oscillation, while the blue and red curves correspond to the oscillation scenarios characterized by Δm_{21}^2 and θ_{12}, based on the best-fit values of KamLAND data and the best-fit values of SK/SNO solar neutrino data, respectively. Our calculations assume ten years of data collection for both LSC at Yemilab and JUNO reactor neutrino experiments. The figure shows that the number of events of reactor neutrinos without oscillation is approximately twenty times higher at JUNO compared to LSC at Yemilab due to the differences in the experimental setup. JUNO, with a reactor power of $26.6\,\mathrm{GW_{th}}$, a 20 kton detector, and a 52.5 km baseline, outperforms LSC at Yemilab, which has a reactor power of $24.8\,\mathrm{GW_{th}}$, a 2 kton detector, and a 65 km baseline.[3] We can see the oscillation behavior of the blue and red solid lines. Note that in the case of no oscillation (black curve), the maximum number of events occurs at the energies around 3–5 MeV. In the right panel of Fig. 1, we can observe that LSC at Yemilab is more sensitive to Δm_{21}^2 because the maximum flavor conversion also occurs around 3–4 MeV, for both KamLAND and SK/SNO best-fit values. On the other hand, for JUNO, the maximum occurs in the energy range of 2–3 MeV, where the number of events is lower by about 30% compared to the SK/SNO best-fit values. Consequently, JUNO demonstrates lower sensitivity compared to Yemilab.

Figure 4 depicts the annual number of solar neutrino events as a function of the electron kinetic energy in LSC at Yemilab, considering the best-fit values of the SK/SNO

data for $\Delta m_{21}^2 = 6.11 \times 10^{-5}$ eV^2 and $\sin^2 \theta_{12} = 0.306$ [39]. The total number of events is represented by the black curve. Additionally, the number of events for the individual solar neutrino components, including pp, ^{7}Be, pep, ^{8}B, hep, ^{15}O, and ^{13}N, are illustrated separately using different colors; dark blue, dark green, brown, red, magenta, light blue, and light green, respectively. This plot provides an overview of the expected event rates for each solar neutrino source, allowing for a detailed analysis of their contributions to the total event count.

In Fig. 5, we have demonstrated the reconstructed number of events as a function of the neutrino energy,
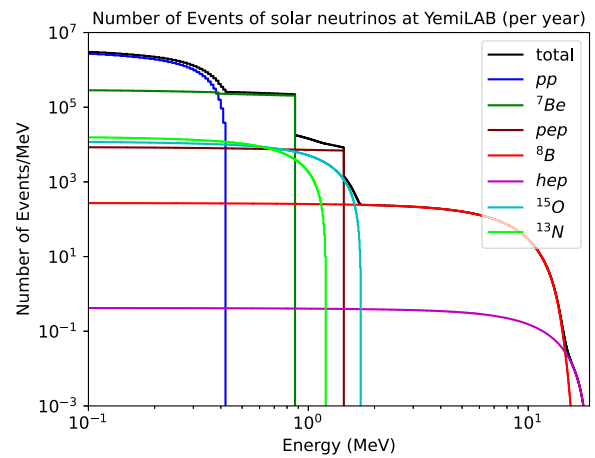

FIG. 4.   The number of events per MeV per year as a function of the kinetic energy of the electron, assuming the best-fit values of SK/SNO solar neutrino data ($\Delta m_{21}^2 = 6.11 \times 10^{-5}$ eV^2 and $\sin^2\theta_{12} = 0.306$), is illustrated. The total number of events is represented by the black curve. The number of events for pp, ^{7}Be, pep, ^{8}B, hep, ^{15}O, and ^{13}N neutrinos are shown separately in dark blue, dark green, brown, red, magenta, light blue, and light green, respectively.

---

[3]The ratio of the number of events at JUNO to LSC at Yemilab without oscillation can be estimated as $(26.6/24.8) \times (20/2) \times (65/52.5)^2$.
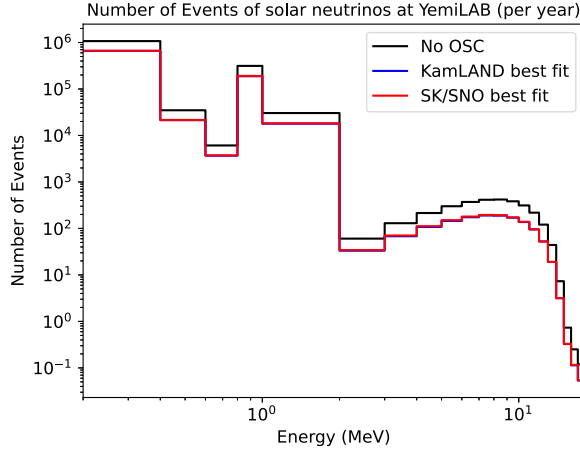
FIG. 5. Number of events per bin per year as a function of neutrino energy for different values of Δm_{21}^2 and θ_{12}, corresponding to the best-fit values of KamLAND data (blue curves) and the best-fit values of SK/SNO solar neutrino data (red curves) and no oscillation (black curve). The number of events in each bin for the best-fit values of KamLAND and solar data are close to each other, therefore, they coincide.

assuming no oscillation number of events (black curve), the best-fit values of KamLAND data (blue curves) and the best-fit values of SK/SNO solar neutrino data (red curves). The number of events in each bin for the best-fit values of KamLAND and SK/SNO solar data are close to each other, compared to the no oscillation case, therefore they coincide for some bins.

The number of events for the solar neutrino data as a function of the electron's kinetic energy is presented in the conceptual design of JUNO [13]. Figure 6–3 of the JUNO conceptual design illustrates two scenarios for the background of low-energy solar data (below 1.8 MeV); one with high background and the other with a reduced lower background assumption based on ideal radiopurity conditions. As mentioned before, at lower energies, JUNO primarily detects ^{7}Be neutrinos, with a small contribution from pp neutrinos. For higher energies, JUNO is capable of detecting ^{8}B neutrinos, as demonstrated in Figure 6–4 of the JUNO conceptual design [13]. Neutron captures on the steel of the detector result in the production of 6 MeV and 8.5 MeV gamma rays, contributing to the external background and reducing the fiducial size of the detector by half. In our analysis on the other hand, we focus on the number of events at JUNO for energies larger than 14.5 MeV. Our results indicate that JUNO, with a 20 kton fiducial volume, is capable of detecting six events of hep neutrinos with electron kinetic energies larger than 14.8 MeV after ten years of data taking. Please note that the energy resolution of SK is given by $\sigma(E) = -0.0839 + 0.349\sqrt{E} + 0.0397E$, which is approximately 2 MeV (13%) at $E = 15$ MeV [45]. Consequently, SK is unable to detect hep neutrinos since the number of hep neutrinos
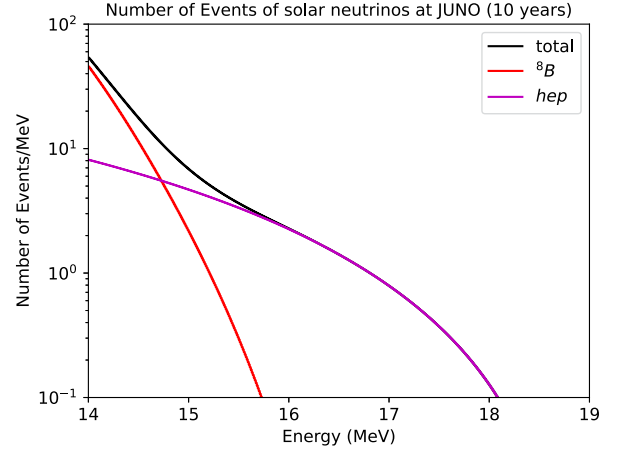

FIG. 6. Number of events per MeV as a function of the kinetic energy of electron for the values of Δm_{21}^2 and θ_{12} fixed at the best-fit values of SK/SNO solar data. We expect six events of hep neutrinos and one event of ^{8}B neutrinos at energies larger than 14.8 MeV after ten years of data taking at JUNO.

drops quickly beyond 17 MeV, as can be seen from Fig. 6. On the other hand, JUNO has a superior energy resolution compared to SK, enabling it to detect hep neutrinos. In our calculations, we have assumed perfect energy resolution for JUNO. We anticipate observing approximately one event from ^{8}B neutrinos within this energy range. It is worth noting that due to neutron captures and a potential reduction in the fiducial volume at these energies, the number of events may be lower. Figure 6 displays the number of events as a function of kinetic energy for energies larger than 14 MeV. Notably, for energies above 14.8 MeV, the number of hep neutrino events exceeds that of ^{8}B neutrinos.

B. Sensitivities on the solar neutrino parameters

In Fig. 7, we show the sensitivities on solar neutrino oscillation parameters θ_{12} and Δm_{21}^2 from solar neutrino detection in LSC at Yemilab and reactor neutrino detection both in LSC at Yemilab and JUNO for 10 years, while fixing oscillation parameters $\delta_{\rm CP} = 0$, Δm_{31}^2 from nu-fit [20], θ_{13} as the best-fit value of Daya Bay [40], assuming normal mass ordering.

As it is shown, we expect the solar neutrino data in LSC at Yemilab can determine the value of θ_{12} with the highest precision, albeit with the smallest size of the fiducial volume among the considerations listed in Table I. The main reason is its low energy threshold along with detection of pp neutrinos and ^{7}Be neutrinos with high statistics with the order of several hundred thousand events per year. Our results show that assuming a fixed standard solar model and in the absence of flux uncertainty, we obtain $\Delta\theta_{12} = 0.02°$. In our calculations, we operate under the assumption that pile-up events become negligible after background rejection. Considering the scenario where the
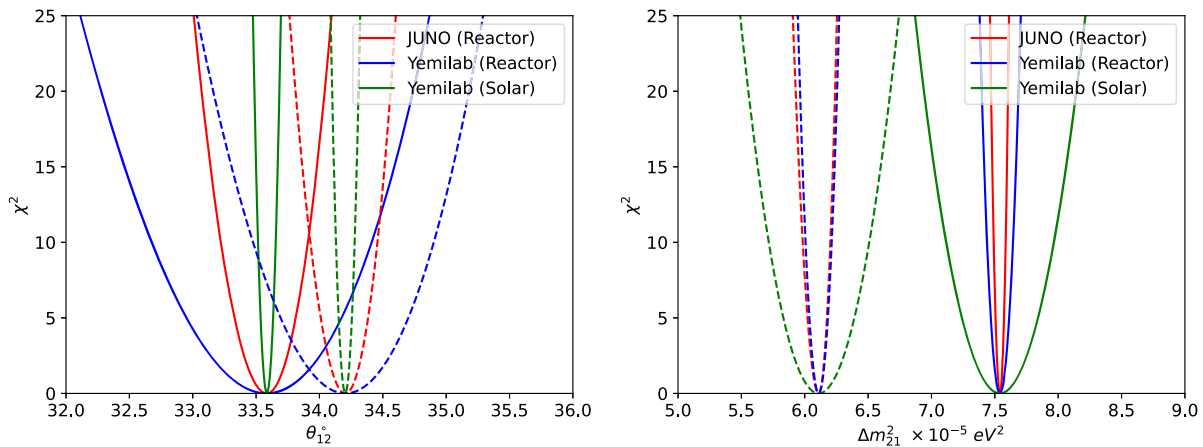
FIG. 7.   The constraints on solar neutrino oscillation parameters θ_{12} and Δm_{21}^2 using detection of solar neutrinos in LSC at Yemilab and detection of reactor neutrinos both in LSC at Yemilab and JUNO for 10 years. The dashed curves are plotted based on the assumption that the best-fit values of SK/SNO solar data are the true value, while the solid curves are plotted assuming the best-fit values of KamLAND as the true value. The blue, red, and green curves correspond to the Yemilab reactor, JUNO, and Yemilab solar data, respectively. As it is demonstrated, solar neutrino in LSC at Yemilab determines the value of θ_{12} with the highest precision. JUNO will determine the value of Δm_{21}^2 with the highest precision.

number of pile-up events is comparable to pp neutrino events after background rejection, accounting solely for statistical uncertainty introduces a change around 10%, which is deemed nonsignificant. Conversely, if we hypothetically assume that pile-up events are ten times more prevalent than pp events, this alters the precision of the measurement by approximately 50% ($\Delta \theta_{12} = 0.03°$). It is important to note that the systematic uncertainty associated with pile-up background, or any reduction in signal efficiency, has the potential to significantly impact the final result.

Neglecting double pile-up ^{14}C background and considering only the flux uncertainty of ^7Be, which $\Delta \Phi_{^7Be}$ is 7%, yields a similar result. This suggests that the determination of θ_{12} remains robust despite uncertainties associated with ^7Be. Considering solely the pp neutrino flux uncertainty, we obtain $\Delta \theta_{12} = 0.04°$, and this result remains robust as long as the total uncertainty of pp neutrinos remains below 1% (accounting for both flux uncertainty and fiducial volume uncertainty). Incorporating both pp and ^7Be neutrino flux uncertainties results in $\Delta \theta_{12} = 0.11°$, and including fiducial volume uncertainties alongside both flux uncertainties leads to $\Delta \theta_{12} = 0.12°$. This result is comparable to the constraint obtained using JUNO reactor neutrinos. However, it is important to note that we have not considered the uncertainties associated with the reactor flux or so-called reactor antineutrino anomaly [46]. Let us remind that up to now we have assumed energy resolution given by $\sigma_E/E \simeq 1/\sqrt{1000E/\text{MeV}}$. Assuming energy resolution of $\sigma_E/E \simeq 1/\sqrt{500E/\text{MeV}}$ leads to $\Delta \theta_{12} = 0.15°$ assuming all flux uncertainties plus fiducial volume uncertainty. Taking into account these uncertainties will potentially weaken the results obtained by JUNO reactor.

Considering reactor neutrino flux uncertainties is beyond the scope of this work.

On the other hand, the detection of the reactor neutrinos has a better sensitivity to determine the value of Δm_{21}^2. JUNO detector with a larger fiducial volume, more powerful reactors and closer baseline can provide a better sensitivity than LSC at Yemilab if Δm_{21}^2 is closer to the KamLAND best-fit value.

We demonstrate the result assuming two cases: (i) the true values of the solar neutrino oscillation parameters are the best-fit values of the reactor neutrino results from KamLAND, (ii) the best-fit values of the SK/SNO solar data as the true values for solar neutrino oscillation parameters. As it is demonstrated in the figure, for larger values of Δm_{21}^2 closer to the best-fit value of KamLAND, JUNO has approximately twice better sensitivity to determine the value of Δm_{21}^2, however, if Δm_{21}^2 is smaller and it is close to the best-fit value of the SK/SNO solar data, the sensitivity of JUNO is comparable with LSC at Yemilab. Later, we will show the potential of these experiments for simultaneous measurement of Δm_{21}^2 and θ_{12}. For smaller values of Δm_{21}^2, closer to the best-fit values of SK/SNO solar data, LSC at Yemilab reactor neutrino will have a better sensitivity to determine Δm_{21}^2 more precisely than JUNO, while for larger values of Δm_{21}^2, close to the best-fit values of KamLAND, JUNO has a better sensitivity to determine Δm_{21}^2, in the presence of θ_{12} or marginalizing over θ_{12}.

In Fig. 8, we show the sensitivities of JUNO on the solar neutrino oscillation parameters θ_{12} and Δm_{21}^2 from the detection of the solar neutrinos. Notice that, due to the large amount of ^{14}C background below 0.15 MeV, only the electron with larger values of kinetic energy can be
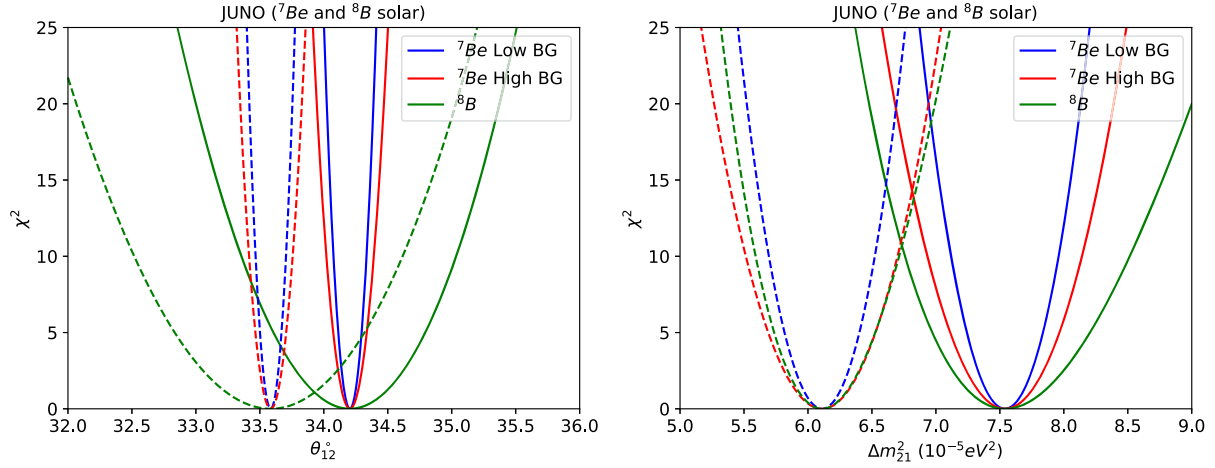
FIG. 8.   The constraints on solar neutrino oscillation parameters θ_{12} and Δm_{21}^2 with detection of solar neutrinos at JUNO, assuming ten years of data collection. The dashed curves are plotted based on the assumption that the best-fit values of SK/SNO solar data is the true value, while the solid curves are plotted assuming the best-fit values of KamLAND as the true value. The green curves correspond to the ^{8}B solar neutrinos detected at JUNO. The blue and red curves are plotted assuming low background and high background for the ^{7}Be neutrinos, respectively. As observed, the solar neutrino detection at JUNO exhibits lower sensitivity in measuring θ_{12} and Δm_{21}^2 compared to the reactor neutrino detection at JUNO and Yemilab, as well as the solar neutrino detection at Yemilab.

detected. For energies larger than 0.15 MeV, there are also other sources of background such as ^{210}Bi and ^{11}C so that JUNO can only detect the ^{7}Be neutrino at low energies. In this case, the background is two times larger than the signal [13]. For the case of ideal radiopurity background, only ^{7}Be neutrinos are detectable and the number of events of the signal is about one order of magnitude larger than the background. Also, the other sources of low energy solar neutrinos will be much smaller than the background. For higher energies, we have a large amount of ^{10}C and ^{11}C background, which are one to two orders of magnitude larger than ^{8}B neutrino events, for energies smaller than 3.5 MeV.

Comparing Figs. 7 and 8, we observe that under the assumption of low background, the constraint on Δm_{21}^2 derived from the ^{7}Be solar data of JUNO is comparable to, but slightly weaker, than that obtained from the solar data of LSC at Yemilab. Note that solar data from both LSC at Yemilab and JUNO can result in weaker constraints on Δm_{21}^2 compared to reactor data. It is worth noting that the constraint obtained using ^{8}B solar data at JUNO is significantly weaker than reactor data of JUNO and Yemilab, and solar data at Yemilab constraints. In obtaining the constraints on Δm_{21}^2, we have fixed the value of θ_{12} as the best-fit values from KamLAND and SK/SNO.

In the determination of θ_{12}, the ^{8}B solar data at JUNO is observed to exhibit less sensitivity compared to the ^{7}Be data. However, when considering the ^{7}Be solar data at JUNO, a constraint on θ_{12} is obtained that is comparable, albeit slightly less sensitive, to the solar data at LSC at Yemilab. It is important to note that the flux uncertainties have not been accounted for in our analysis. Including these

uncertainties would lead to weakened constraints, especially for the solar data at JUNO, as ^{7}Be and ^{8}B neutrinos are associated with significant theoretical flux uncertainties. In our analysis for determining θ_{12}, we have fixed the value of Δm_{21}^2 as the best-fit values from KamLAND and SK/SNO.

Nevertheless, the detection of solar neutrinos at JUNO will play key roles in determining the individual fluxes of ^{7}Be and ^{8}B as well as their ratio. Moreover, the detection of *hep* neutrinos and their flux measurement will be another astonishing potential of JUNO as it is demonstrated in Fig. 6. We expect the combination of JUNO and LSC at Yemilab solar neutrinos can open a new window to study the structure of the Sun by precise measurements of all the solar neutrino fluxes and their ratios.

It is important to emphasize that the primary goal of JUNO is the determination of the neutrino mass ordering, and its baseline is optimized for this purpose. Additionally, if the value of Δm_{21}^2 is close to the best-fit value determined by KamLAND, JUNO can provide a highly precise measurement of Δm_{21}^2. However, for smaller values of Δm_{21}^2, a longer baseline is more effective. It is worth noting that JUNO benefits from a ten times larger detector, reactor power that is one and a half times greater, and a flux that is $(65 \text{ km}/52.5 \text{ km})^2$ higher due to the closer baseline.

In Fig. 9, we illustrate the sensitivities of JUNO and LSC at Yemilab in determining the value of Δm_{21}^2 from detecting the reactor neutrinos. The 1σ confidence level intervals are shown for different values of Δm_{21}^2. The solid line represents a fixed value of θ_{12} to the best-fit values of KamLAND, while the dashed line represents the 1σ interval obtained through marginalization over θ_{12} and θ_{13}.
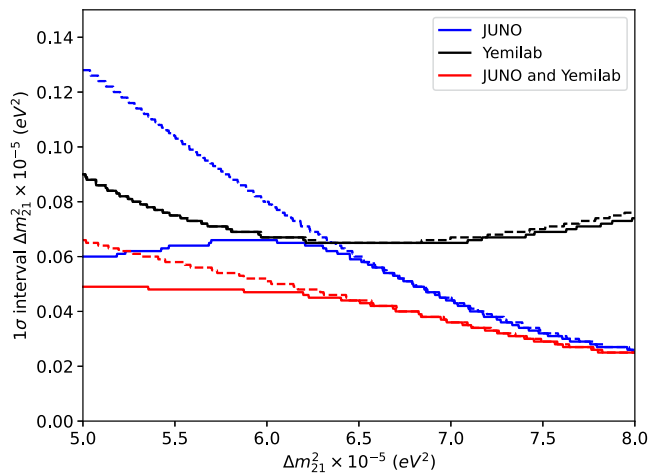
FIG. 9. The one sigma interval that JUNO and LSC at Yemilab can achieve for different values of Δm_{21}^2 after ten years of reactor neutrino data taking. As shown, for smaller values of Δm_{21}^2, JUNO has less sensitivity to determine Δm_{21}^2, and its precision will be closer to that of Yemilab. However, JUNO exhibits better sensitivity for larger values of Δm_{21}^2. Dashed curves are plotted when marginalizing over θ_{12} and θ_{13}. The solid curves are plotted setting all oscillation parameters to their best-fit values [20,39,40].

To draw the dashed line, we marginalized over θ_{12} and θ_{13} and treated both of these parameters as pull terms. Additionally, we conducted another analysis by fixing θ_{13} to the best-fit value reported in the Daya Bay experiment [40], comparing the results to those presented in Fig. 9. The results were similar in both cases.

As demonstrated, for larger values of Δm_{21}^2, JUNO exhibits two times better sensitivity in determining Δm_{21}^2 compared to LSC at Yemilab. On the other hand, for smaller values of Δm_{21}^2, LSC at Yemilab shows a better sensitivity. It should be noted that despite the similar flux shape and cross sections of neutrinos from the reactors, the different baselines result in distinct neutrino oscillation probability patterns and, consequently, different patterns of events per energy bin. Notably, when considering $\Delta m_{21}^2 < 6.4 \times 10^{-5}$ and assuming marginalization over θ_{12}, the reactor neutrino detection in LSC at Yemilab demonstrates superior sensitivity for measuring Δm_{21}^2. Moreover, the determination of Δm_{21}^2 using reactor neutrinos with two different baselines helps in reducing the systematic uncertainties associated with the reactor neutrino flux or other sources of systematic uncertainties of the quantities such as θ_{12} and backgrounds. Notice that the result from Yemilab is robust when considering the marginalization of θ_{12} since the minimum of P_{ee} or the maximum flavor conversion occurs within the energy range where the largest number of events is observed (Fig. 1). Therefore, if the true value of Δm_{21}^2 is 6.11×10^{-5} eV^2, we will have a better sensitivity to both θ_{12} and Δm_{21}^2. However, this is not the case for JUNO, as the maximum flavor conversion occurs around

the energy range of 2–3 MeV where the number of events is lower around 30%. As a result, a strong anti-correlation is present between θ_{12} and Δm_{21}^2 in the case of JUNO.

We have also studied the potential of LSC at Yemilab to determine the mass ordering, which is sensitive to the energy resolution of the detector. After ten years of data taking, LSC at Yemilab will determine the mass ordering with 1σ C.L. for $5\%\sqrt{E}$, $4\%\sqrt{E}$ energy resolution and 2σ C.L. for $3\%\sqrt{E}$ energy resolution. On the other hand, the sensitivity of more dedicated experiment JUNO is beyond 5σ C.L. after five years of data taking with the energy resolution of the detector ranging from $3\%\sqrt{E}$ to $3.5\%\sqrt{E}$. Note that, the true value of the solar oscillation parameters Δm_{21}^2 and θ_{12} can affect determination of mass ordering by JUNO [47].

Figure 10 shows the simultaneous measurement of Δm_{21}^2 and θ_{12} using solar neutrino detection at JUNO for 10 years. The figure presents two distinct scenarios; a low background case (upper panels) and a high background case (middle panels). In the left panels, we assume the fixed value of θ_{12} to be the best-fit value obtained from KamLAND, while in the right panels, we fix it as the best-fit value derived from SK/SNO. The dashed curves correspond to the ^{8}B solar data, while the dotted curves correspond to the ^{7}Be solar data. The solid contours correspond to the combined data of ^{7}Be and ^{8}B solar data. As can be observed, the ^{8}B data exhibits sensitivity to the simultaneous measurement of Δm_{21}^2 and θ_{12} due to the significant impact of the resonance effect within its energy range. However, as previously mentioned, the oscillation probability of ^{7}Be monochromatic solar neutrinos shows an anti-correlated dependence on θ_{12} and Δm_{21}^2. This behavior can be observed from Eq. (6), particularly for small values of ϵ_{12}, where $\cos 2\theta_{12}^m \sim \cos 2\theta_{12} - \frac{A_{CC}}{\Delta m_{21}^2}$, aligning with our expectations for an anti-correlated relationship. By combining both the ^{8}B and ^{7}Be solar data obtained at JUNO, a more stringent constraint can be achieved. Notice that when considering the sensitivity of solely ^{8}B solar data, its constraints are considerably weaker in comparison to JUNO reactor data, as well as solar and reactor data from LSC at Yemilab. Thus, detecting only ^{8}B neutrinos will not lead to a significant constraint. In the top and middle panels, we have not included the flux uncertainty of the solar neutrinos as well as the other systematics. However, it is worth mentioning that in the case of pp neutrinos which could be detected at LSC, the flux uncertainty is very small, approximately 0.6% [42]. This robustly supports our result for LSC at Yemilab, as including the pp flux uncertainty would not significantly change our conclusion that LSC will provide the best sensitivity for measuring θ_{12}.[4] On the other hand, the flux uncertainty for ^{7}Be and ^{8}B neutrinos is

---

[4]Note, however, that a more dedicated analysis of estimating other possible systematic uncertainties at LSC is required.
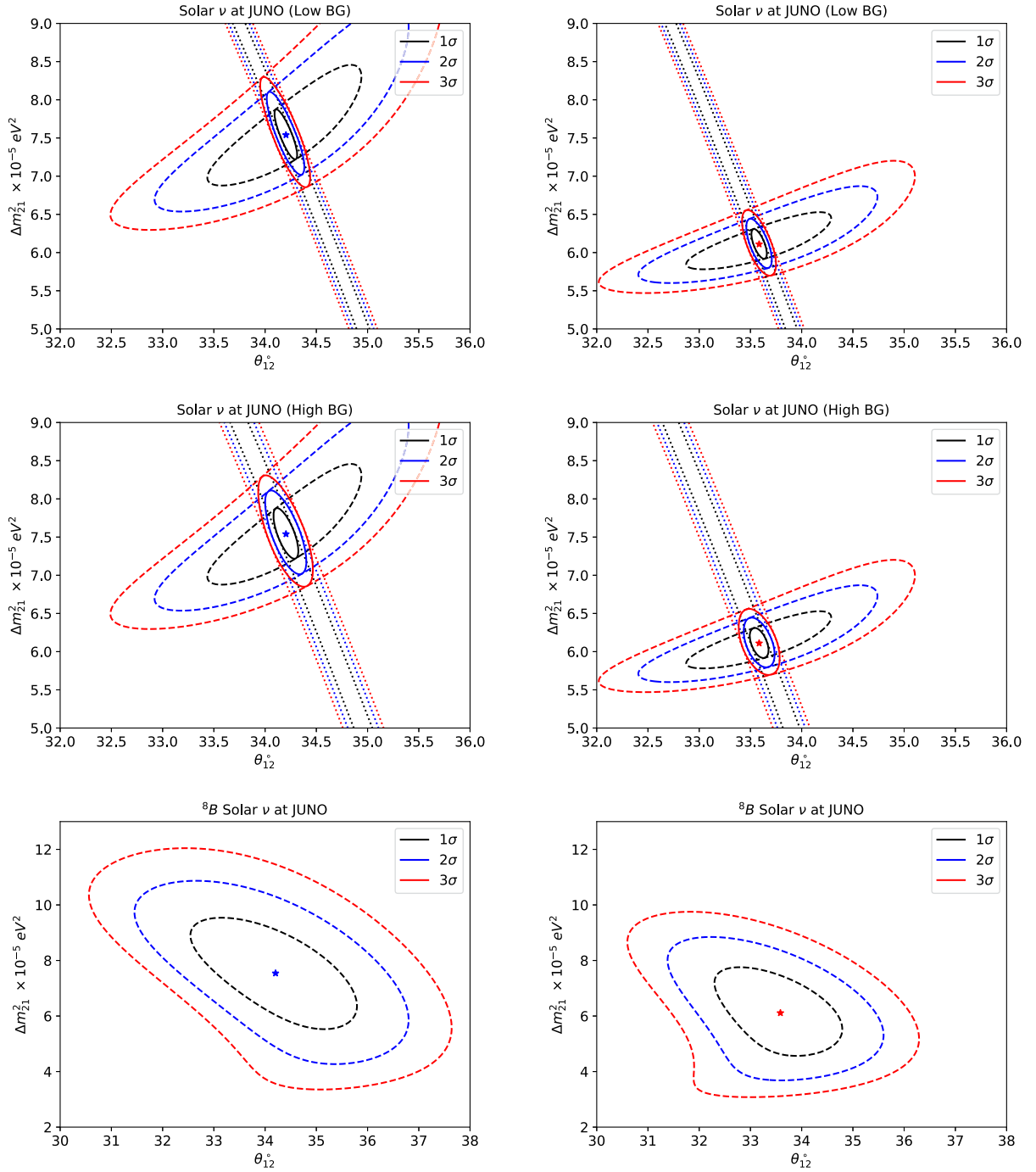
FIG. 10. Simultaneous measurement of Δm_{21}^2 and θ_{12} using solar neutrino detection at JUNO, assuming ten years of data collection, with low (upper panels) and high (middle panels) background levels considering the best-fit values of KamLAND (left panels) and SK/ SNO (right panels). The dashed and dotted curves correspond to the ^{8}B and ^{7}Be neutrinos, respectively. The solid curves represent the combination of ^{8}B and ^{7}Be neutrinos. The bottom panel indicates the constraint obtained considering only ^{8}B including 3.5% flux uncertainty. As can be observed, including the flux uncertainty will wash out the sensitivity.

7% and 12%, respectively, implying that including these uncertainties will weaken the obtained constraint on JUNO solar neutrinos. In the bottom panels, we are showing the simultaneous measurement of Δm_{21}^2 and θ_{12} using ^{8}B solar neutrino detection at JUNO with including 3.5% flux

uncertainty. We have chosen this value for flux uncertainty to compare our results with that of Ref. [38] and we find that our results are in agreement with theirs. Note that 14 different systematics is included in the analysis performed in Ref. [38], while only the flux uncertainty systematic is
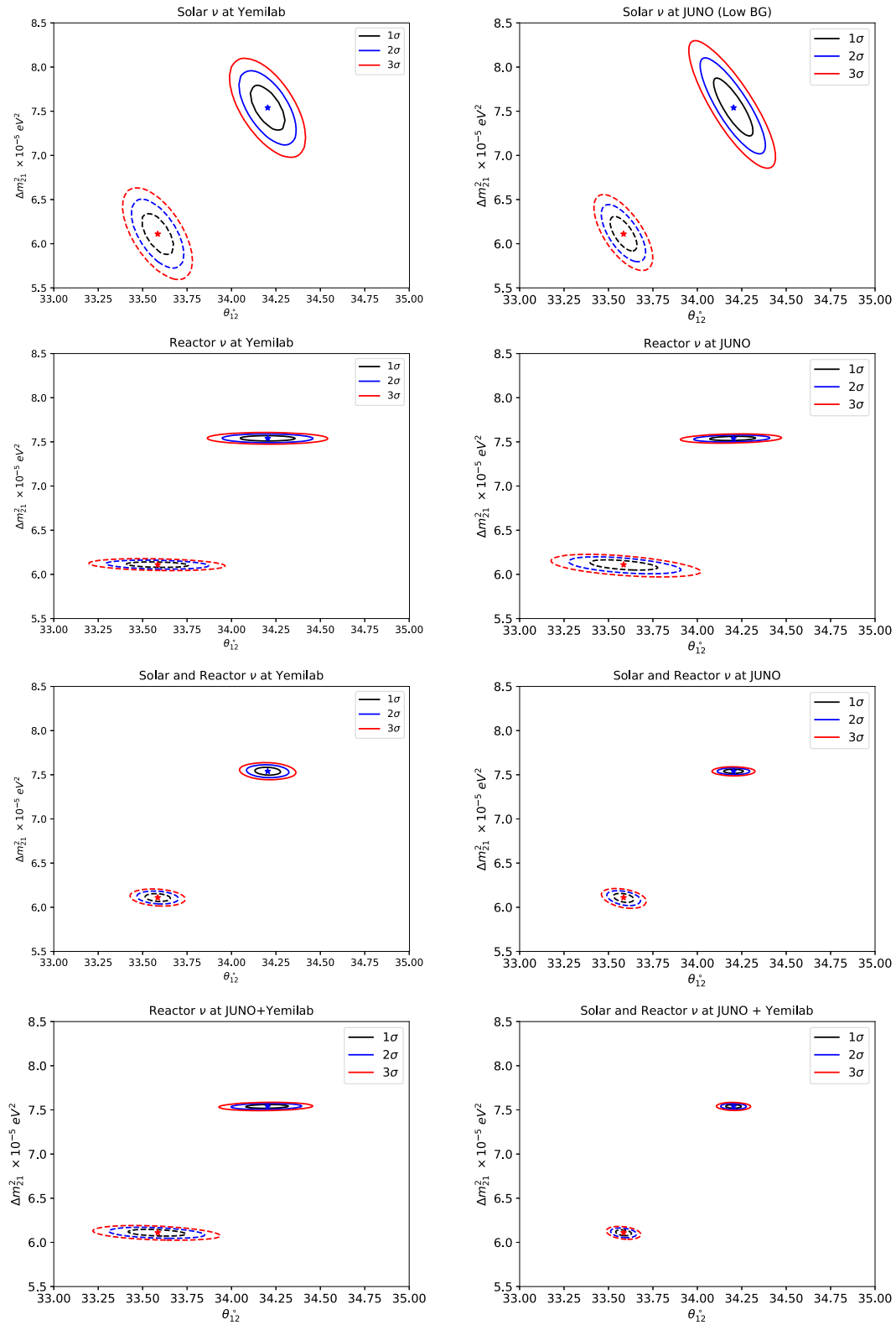
FIG. 11.   Simultaneous measurement of θ_{12} and Δm_{21}^2 can be achieved through the detection of solar and reactor neutrinos at Yemilab, as well as the detection of reactor neutrinos at JUNO. Additionally, combining the data from both experiments can improve the sensitivity.

included in the lower panels of Fig. 10. As observed, including the flux uncertainty can significantly relax the constraint. In the same way, including other systematics can wash out the sensitivity of JUNO to the ^{8}B solar neutrino detection.

For JUNO, the inclusion of ^{7}Be uncertainty diminishes the sensitivity for the simultaneous measurement of θ_{12} and Δm_{21}^2. Consequently, combining the constraints from ^{7}Be and ^{8}B detection does not alter the results and remains approximately the same as the bottom panel of Fig. 10. References [48,49] present comparable results with ours. Our study provides a more stringent constraint as these references have incorporated more systematics. Moreover, Ref. [50] investigates the sensitivity of JUNO to various solar models and the flux measurement of the CNO cycle, ^{7}Be, and pep neutrinos, which is crucial for studying solar characteristics.

Figure 11 demonstrates the sensitivities of LSC at Yemilab and JUNO to simultaneous measurement of θ_{12} and Δm_{21}^2. For the true values of θ_{12} and Δm_{21}^2, we have assumed two cases: the best-fit values of KamLAND and that of SK/SNO solar data, as stated earlier. In the top panels, we show the sensitivity of LSC at Yemilab (left) and JUNO (right) using ten years of solar data only. We have included the low background for JUNO here which leads to a more stringent constraint compared to the high background case. In the second row, the sensitivity at LSC at Yemilab (right) and JUNO (left) using ten years of reactor data is demonstrated. In the panel on the right side of the third row, the expected sensitivity of LSC at Yemilab is displayed after combining both solar and reactor data. The panel on the left side of the third row represents the combined solar and reactor data at JUNO. It can be observed that the results of combining solar and reactor data at LSC at Yemilab are comparable to those of JUNO. However, it should be noted that the inclusion of flux uncertainty and high background for JUNO has the potential to weaken the obtained constraint.

Noticeably, solar neutrino detection by LSC at Yemilab can determine the value of θ_{12} with the highest precision. For the simultaneous measurement of θ_{12} and Δm_{21}^2, LSC at Yemilab with the detection of both solar and reactor neutrinos will be comparable with or better than JUNO with reactor neutrinos only. Note that in the case of using reactor neutrinos only, LSC at Yemilab shows a comparable sensitivity on Δm_{21}^2 for the SK/SNO best-fit values ($\Delta m_{21}^2 = 6.11 \times 10^{-5}$ eV^2 and $\sin^2 \theta_{12} = 0.306$ [39]), while for the other case, JUNO has a better sensitivity to determine the value of Δm_{21}^2. In the bottom panels, we show the combined sensitivity: with the reactor neutrino data only (left) and both the solar and reactor neutrino data from LSC at Yemilab and reactor data from JUNO (right). Remarkably, we expect that the combination of LSC in Yemilab and JUNO can determine the parameters θ_{12} and Δm_{21}^2 with a sub-percent precision level. Comparing the bottom-left and right panels, we can see the important contribution of solar neutrino detection in LSC at Yemilab in improving precision.

VI. CONCLUSIONS

We have explored the sensitivities of LSC at Yemilab and JUNO to solar neutrino oscillation parameters θ_{12} and Δm_{21}^2. In our analysis, we have included both reactor and solar data of the reference experiments. For LSC at Yemilab (reactor), we have considered a fiducial volume of 2 kton, while for the JUNO reactor, a fiducial volume of 20 kton has been taken into account [38]. In the case of solar neutrinos, we have used a 1 kton fiducial volume for LSC at Yemilab, and for JUNO, we have considered a fiducial volume of 20 kton for ^{7}Be and hep neutrinos, and 16 kton for ^{8}B neutrinos (table I). We reconstructed the number of events per bin as a function of energy for reactor detectors of JUNO and Yemilab assuming $\Delta m_{21}^2 = 7.54 \times 10^{-5}$ eV^2 (blue) and $\Delta m_{21}^2 = 6.11 \times 10^{-5}$ eV^2 (red) in Fig. 3 assuming 10 years of data taking for each experiment. We observed that the oscillation pattern differs between the reference experiments due to the difference in their baselines. This difference holds the potential to enhance the sensitivity in measuring Δm_{21}^2.

Overall, we have demonstrated the excellent potential of LSC at Yemilab in determining the solar neutrino parameter θ_{12} from detecting solar neutrinos due to the large number of events that can be attributed to low energy threshold, suppressed number of background, and detection of pp neutrinos (Fig. 7). We have investigated the impact of detecting ^{7}Be solar neutrinos on the determination of θ_{12}. Let us emphasize that the detection of solely ^{8}B neutrinos provides limited accuracy (Fig. 10). However, by combining the ^{8}B data with ^{7}Be data, the sensitivity can be enhanced to a level comparable to that of LSC at Yemilab. It is important to note that both ^{7}Be and ^{8}B neutrinos have large flux uncertainties. Furthermore, we have not included the systematic uncertainties of the background. In particular, the systematic uncertainty associated with double pile-up events can be substantial. Moreover, any reduction in pile-up event discrimination capabilities could reduce the sensitivity to pp neutrinos.

Combined with the reactor neutrino data coming from the Hanul power plant, LSC at Yemilab we can simultaneously determine the solar neutrino parameters θ_{12} and Δm_{21}^2 to a percent level (Fig. 11). On the other hand, the reactor neutrino detection in JUNO can precisely determine Δm_{21}^2, in particular for the best-fit value from KamLAND. Furthermore, for smaller values of Δm_{21}^2, particularly for the best-fit value obtained from solar data at SK/SNO, LSC at Yemilab exhibits superior capability in determining the precise value of Δm_{21}^2 compared to JUNO (Fig. 9). It is intriguing that the combination of all of those observations, i.e., the solar with reactor data in LSC at Yemilab and the reactor data in JUNO, renders us to simultaneously

determine the parameters θ_{12} and Δm_{21}^2 with subpercent level precision for both cases of the best-fit values of KamLAND and SK/SNO. We expect such precise determination of the solar neutrino parameters can shed light in probing new physics beyond the SM as well as understanding the neutrino flux and the details of the dynamics of the Sun and the reactors.

[1] B. T. Cleveland, T. Daily, R. Davis, Jr., J. R. Distel, K. Lande, C. K. Lee, P. S. Wildenhain, and J. Ullman, Astrophys. J. **496,** 505 (1998).

[2] J. Hosaka *et al.* (Super-Kamiokande Collaboration), Phys. Rev. D **73,** 112001 (2006).

[3] J. P. Cravens *et al.* (Super-Kamiokande Collaboration), Phys. Rev. D **78,** 032002 (2008).

[4] K. Abe *et al.* (Super-Kamiokande Collaboration), Phys. Rev. D **83,** 052010 (2011).

[5] F. Kaether, W. Hampel, G. Heusser, J. Kiko, and T. Kirsten, Phys. Lett. B **685,** 47 (2010).

[6] J. N. Abdurashitov *et al.* (SAGE Collaboration), Phys. Rev. C **80,** 015807 (2009).

[7] B. Aharmim *et al.* (SNO Collaboration), Phys. Rev. C **88,** 025501 (2013).

[8] A. Gando *et al.* (KamLAND Collaboration), Phys. Rev. D **88,** 033001 (2013).

[9] L. Wolfenstein, Phys. Rev. D **17,** 2369 (1978).

[10] S. P. Mikheyev and A. Y. Smirnov, Sov. J. Nucl. Phys. **42,** 913 (1985).

[11] S. P. Mikheev and A. Y. Smirnov, Nuovo Cimento Soc. Ital. Fis. **9C,** 17 (1986).

[12] M. Agostini *et al.* (BOREXINO Collaboration), Nature (London) **587,** 577 (2020).

[13] F. An *et al.* (JUNO Collaboration), J. Phys. G **43,** 030401 (2016).

[14] P. B. Denton and J. Gehrlein, J. High Energy Phys. 06 (2023) 090.

[15] P. Bakhti and M. Rajaee, Phys. Rev. D **102,** 035024 (2020).

[16] J. Kersten and A. Y. Smirnov, Eur. Phys. J. C **76,** 339 (2016).

[17] M. Maltoni and A. Y. Smirnov, Eur. Phys. J. A **52,** 87 (2016).

[18] P. Bakhti and A. Y. Smirnov, Phys. Rev. D **101,** 123031 (2020).

[19] A. Ioannisian, A. Smirnov, and D. Wyler, Phys. Rev. D **96,** 036005 (2017).

[20] I. Esteban, M. C. Gonzalez-Garcia, M. Maltoni, T. Schwetz, and A. Zhou, J. High Energy Phys. 09 (2020) 178.

[21] F. P. An *et al.* (Daya Bay Collaboration), Phys. Rev. Lett. **108,** 171803 (2012).

[22] J. K. Ahn *et al.* (RENO Collaboration), Phys. Rev. Lett. **108,** 191802 (2012).

[23] H. de Kerret *et al.* (Double Chooz Collaboration), Nat. Phys. **16,** 558 (2020).

[24] S.-H. Seo and S. J. Parke, Phys. Rev. D **99,** 033012 (2019).

[25] A. Hernandez-Cabezudo, S. J. Parke, and S.-H. Seo, Phys. Rev. D **100,** 113008 (2019).

[26] S.-H. Seo *et al.,* arXiv:2309.13435.

[27] P. Huber, M. Lindner, T. Schwetz, and W. Winter, Nucl. Phys. **B665,** 487 (2003).

[28] P. Huber, M. Lindner, and W. Winter, Comput. Phys. Commun. **167,** 195 (2005).

[29] P. Huber, J. Kopp, M. Lindner, M. Rolinec, and W. Winter, Comput. Phys. Commun. **177,** 432 (2007).

[30] J. F. Beacom *et al.* (Jinping Collaboration), Chin. Phys. C **41,** 023002 (2017).

[31] G. Bellini *et al.* (BOREXINO Collaboration), Nature (London) **512,** 383 (2014).

[32] G. Alimonti *et al.* (Borexino Collaboration), Phys. Lett. B **422,** 349 (1998).

[33] L. Bieger *et al.,* Eur. Phys. J. C **82,** 779 (2022).

[34] G.-M. Chen, X. Zhang, Z.-Y. Yu, S.-Y. Zhang, Y. Xu, W.-J. Wu, Y.-G. Wang, and Y.-B. Huang, Nucl. Sci. Tech. **34,** 137 (2023).

[35] P. Bakhti and Y. Farzan, J. High Energy Phys. 07 (2014) 064.

[36] P. Bakhti and Y. Farzan, J. High Energy Phys. 10 (2013) 200.

[37] M. Grassi, J. Evslin, E. Ciuffoli, and X. Zhang, J. High Energy Phys. 09 (2014) 049.

[38] A. Abusleme *et al.* (JUNO Collaboration), Chin. Phys. C **45,** 023004 (2021).

[39] Y. Nakajima, Recent results and future prospects from Super-Kamiokande Creators (2020), 10.5281/zenodo .3959640.

[40] D. Adey *et al.* (Daya Bay Collaboration), Phys. Rev. Lett. **121,** 241805 (2018).

[41] J. N. Bahcall, A. M. Serenelli, and S. Basu, Astrophys. J. Lett. **621,** L85 (2005).

[42] N. Vinyoles, A. M. Serenelli, F. L. Villante, S. Basu, J. Bergström, M. C. Gonzalez-Garcia, M. Maltoni, C. Peña Garay, and N. Song, Astrophys. J. **835,** 202 (2017).

[43] A. Serenelli, Eur. Phys. J. A **52,** 78 (2016).

[44] M. Agostini *et al.* (BOREXINO Collaboration), Nature (London) **562**, 505 (2018).

[45] K. Abe *et al.* (Super-Kamiokande Collaboration), Phys. Rev. D **94**, 052010 (2016).

[46] G. Mention, M. Fechner, T. Lasserre, T. A. Mueller, D. Lhuillier, M. Cribier, and A. Letourneau, Phys. Rev. D **83**, 073006 (2011).

[47] D. V. Forero, S. J. Parke, C. A. Ternes, and R. Z. Funchal, Phys. Rev. D **104**, 113004 (2021).

[48] J. Zhao *et al.* (JUNO Collaboration), arXiv:2210.08437.

[49] A. Abusleme *et al.* (JUNO Collaboration), Prog. Part. Nucl. Phys. **123**, 103927 (2022).

[50] A. Abusleme *et al.* (JUNO Collaboration), J. Cosmol. Astropart. Phys. 10 (2023) 022.